PAPER Special Section on Analog Circuit Techniques and Related Topics

Analytical Expression Based Design of a Low-Voltage FD-SOI CMOS Low-Noise Amplifier

Takao KIHARA[†a)], **Guechol KIM**[†], **Masaru GOTO**[†], **Keiji NAKAMURA**[†], ***Nonmembers***, **Yoshiyuki SHIMIZU**[†], ***Student Member***, **Toshimasa MATSUOKA**[†], ***and*** **Kenji TANIGUCHI**[†], ***Members***

SUMMARY We propose a design methodology of a low-voltage CMOS low-noise amplifier (LNA) consisting of a common-source and a common-gate stages. We first derive equations of power gain, noise figure (NF) and input third-order intercept point (IIP_3) of the two-stage LNA. A design methodology of the LNA is presented by using graphs based on analytical equations. A 1-V 5.4-GHz LNA was implemented in 0.15-μm fully-depleted silicon-on-insulator (FD-SOI) CMOS technology. Measurement results show a power gain of 23 dB, NF of 1.7 dB and IIP_3 of −6.1 dBm with a power consumption of 8.3 mW. These measured results are consistent with calculated results, which ensures the validity of the derived equations and the proposed design methodology.

key words: *low-noise amplifier (LNA), FD-SOI CMOS, noise, linearity, low-voltage*

1. Introduction

Recently, the supply voltage of integrated circuits has been reduced because of MOSFET miniaturization and the increasing demand for low power consumption. It is, however, difficult to realize a radio-frequency (RF) circuit with desired performance at low supply voltage. Promising solutions are two-folds; to develop circuit topologies suitable for low supply voltage and to design circuits in a new process such as the silicon-on-insulator (SOI) process [1], [2].

The first building block of a wireless receiver is the low-noise amplifier (LNA) which amplifies small signals received by an antenna. It has to keep the internal noise as low as possible and to have sufficient high power gain. LNA also requires good linearity to reduce distortion [3], [4]. Considering both low noise and high linearity, it is difficult to design a cascode LNA [5], [6] operating below 1-V supply voltage, although the design methodology of a 2.5-V cascode LNA [7] has been reported.

We investigate the structure of a low-voltage LNA and proposes a new design methodology of the LNA taking power gain, noise and linearity into account. We implement a 1-V 5.4-GHz LNA in 0.15-μm fully-depleted SOI (FD-SOI) CMOS technology and verify both its performance and our design methodology.

This paper is organized as follows. Section 2 describes the circuit topology of a low-voltage LNA. Section 3 shows the small-signal equivalent circuit of the LNA and Sect. 4 derives equations of power gain, noise figure (NF) and input third-order intercept point (IIP_3) of the LNA. Section 5 presents the design methodology. Section 6 shows the measurement results of the fabricated LNA.

Manuscript received June 19, 2006.
Manuscript revised September 7, 2006.
Final manuscript received October 5, 2006.

[†]The authors are with the Department of Electrical, Electronics and Information Engineering, Graduate School of Engineering, Osaka University, Suita-shi, 565–0871 Japan.
a) E-mail: kihara@si.eei.eng.osaka-u.ac.jp

DOI: 10.1093/ietfec/e90–a.2.317

2. Two-Stage LNA

Figure 1 shows a conventional cascode LNA with inductive source degeneration [5], [6] which is widely used as a CMOS LNA. The overdrive voltage of the transistor M_i is expressed as

$$V_{odi} = V_{gsi} - V_{thi} \tag{1}$$

where V_{gsi} and V_{thi} are the gate-source voltage and threshold voltage of M_i, respectively. It is difficult to use this cascode LNA at low supply voltage because the supply voltage must exceed two overdrive voltages, $V_{od1} + V_{od2}$.

In this study, we adopt a two-stage LNA consisting of a common-source and a common-gate stages [8] as shown in Fig. 2. The ac-coupling capacitor C_c is placed between the input and output stages. The two internal LC tanks L_1/C_1 and L_2/C_2 are chosen to resonate at the operation frequency. The transistor M_2 improves reverse isolation and reduces the Miller effect. The minimum supply voltage of the LNA is only V_{od1}, so that the LNA operates at lower supply voltage than the conventional cascode LNA.

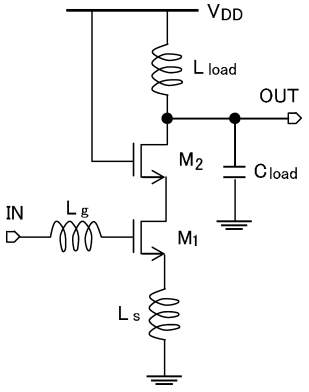

Fig. 1 Schematic of conventional cascode LNA.

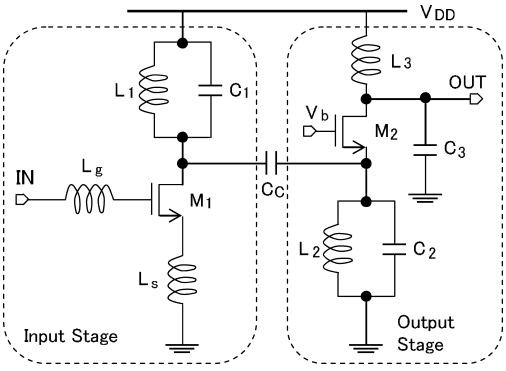

Fig. 2 Schematic of two-stage LNA studied.

3. Small-Signal Equivalent Circuit of the LNA

Figure 3 shows the input stage of the two-stage LNA, where v_s and R_s are a signal source voltage and signal source impedance, respectively. For more precise derivations than those reported in [7], we take account of a parasitic capacitance C_p originating from both the input pad capacitance and gate-drain capacitance of M_1, C_{gd1} [4]. $R_{eq} + j\omega_0 L_{eq}$ denotes the equivalent source impedance looking into the left hand side of the reference plane 2, which is given by

$$R_{eq} = \frac{R_s}{\omega_0^2 C_p^2 R_s^2 + (1 - \omega_0^2 C_p L_g)^2}, \tag{2}$$

$$L_{eq} = \frac{L_g - C_p(\omega_0^2 L_g^2 + R_s^2)}{\omega_0^2 C_p^2 R_s^2 + (1 - \omega_0^2 C_p L_g)^2}. \tag{3}$$

Figure 4 shows the small-signal equivalent circuit of the input stage with the equivalent signal source impedance. Note that an SOI MOSFET has no body effect in the equivalent circuit. The equivalent signal source voltage $v_{s,eq}$ is given by

$$v_{s,eq} = \frac{v_s}{1 - \omega_0^2 C_p L_g + j\omega_0 C_p R_s}. \tag{4}$$

The effective gate-source capacitance of M_1, $C_{gs1,eff}$, effective inductance, $L_{s,eff}$, and non-quasi-static (NQS) resistance, $r_{nqs,eff}$, are expressed as follows [4]:

$$C_{gs1,eff} = (1 + M\alpha_{gd})C_{gs1}, \tag{5}$$

$$L_{s,eff} = \frac{L_s}{1 + M\alpha_{gd}}, \tag{6}$$

$$r_{nqs,eff} = \frac{r_{nqs}}{1 + M\alpha_{gd}}, \tag{7}$$

$$M = g_{m1} \times \left(\frac{1}{g_{m2}} // R_I\right) = \frac{g_{m1} R_I}{1 + g_{m2} R_I}, \tag{8}$$

$$\alpha_{gd} = \frac{C_{gd}}{C_{gs}} \tag{9}$$

where g_{mi} is the transconductance of M_i, M the Miller factor and R_I the parallel resistance of $R_{L_1,p}$ and $R_{L_2,p}$. $R_{L_i,p}$ is the

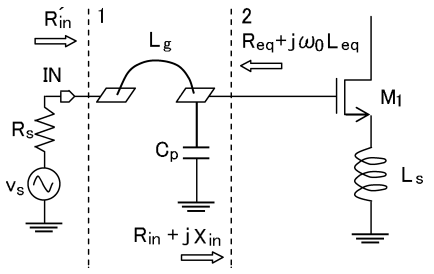

Fig. 3 Input stage of LNA.

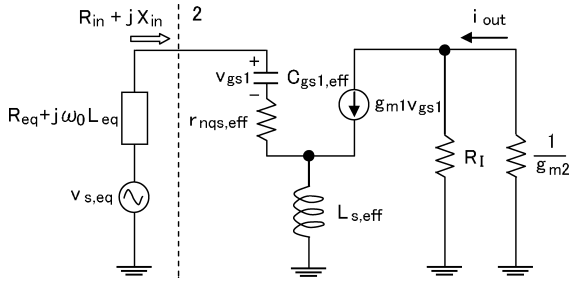

Fig. 4 Small-signal equivalent circuit of input stage.

equivalent resistance of the internal and load LC tanks consisting L_i and C_i (i =1, 2, 3) at a resonant frequency, which is given by

$$R_{L_i,p} \simeq \frac{\omega_0^2 L_i^2}{R_{L_i,s}} \tag{10}$$

where $R_{L_i,s}$ is the series resistance of L_i. From Eqs. (5)–(9), the real and imaginary parts of the input impedance looking into the right hand side of the reference plane 2 are given by

$$R_{in} = r_{nqs,eff} + \omega_{T1} L_{s,eff}, \tag{11}$$

$$X_{in} = \omega_0 L_{s,eff} - \frac{1}{\omega_0 C_{gs1,eff}} \tag{12}$$

where $\omega_{Ti} = g_{mi}/C_{gsi}$. R'_{in} denotes the input impedance of the LNA looking into the right hand side of the reference plane 1, which is given by

$$R'_{in} = \frac{R_{in}(1 - \omega_0^2 L_g C_p) + j(\omega_0 L_g + X_{in} - \omega_0^2 L_g C_p X_{in})}{1 - \omega_0 C_p X_{in} + j\omega_0 C_p R_{in}}. \tag{13}$$

From Fig. 4, the impedance matching condition is given by

$$R'_{in} = R_s \tag{14}$$

or

$$R_{eq} = R_{in}, \tag{15}$$

$$\omega_0 L_{eq} = -X_{in}. \tag{16}$$

4. Power Gain, NF and IIP$_3$ of Two-Stage LNA

For our design optimization, we derive expressions of power gain, NF and IIP$_3$ of the two-stage LNA.

4.1 Power Gain

The output power of the LNA is given by the output load $R_{L_3,p}$ and the current injected in the load i_{out} as

$$P_{out} = |i_{out}|^2 R_{L_3,p} \tag{17}$$

where $R_{L_3,p}$ is given by Eq. (10). Based on the equivalent circuit shown in Fig. 4, $|i_{out}|^2$ is given by

$$|i_{out}|^2 = \frac{4P_{av}R_{eq}}{(R_{eq}+R_{in})^2}\left(\frac{\omega_{T1}}{\omega_0}\right)^2\left(\frac{R_I}{R_I+1/g_{m2}}\right)^2 \tag{18}$$

where P_{av} is the available power of the source.

$$P_{av} = \frac{|v_{s,eq}|^2}{4R_{eq}} = \frac{|v_s|^2}{4R_s}. \tag{19}$$

From Eqs. (17)–(19), the power gain of the two-stage LNA is derived as

$$G_t = \frac{4R_{eq}R_{L_3,p}}{(R_{eq}+R_{in})^2}\left(\frac{\omega_{T1}}{\omega_0}\right)^2\left(\frac{R_I}{R_I+1/g_{m2}}\right)^2. \tag{20}$$

4.2 NF

Figure 5 shows the noise equivalent circuit of input stage of the LNA. The noise voltage, $v_{ns,eq}$, the drain noise and the induced-gate noise currents, i_{ndi} and i_{ngi}, of M_i (i = 1, 2) are expressed as

$$\overline{|v_{ns,eq}|^2} = 4k_BTR_{eq}\Delta f, \tag{21}$$

$$\overline{|i_{ndi}|^2} = 4k_BT\frac{\gamma_i}{\alpha_i}g_{mi}\Delta f, \tag{22}$$

$$\overline{|i_{ngi}|^2} = 4k_BT\delta_i\frac{(\omega C_{gsi})^2}{\kappa_i g_{d0i}}\Delta f \tag{23}$$

where $\alpha_i = g_{mi}/g_{d0i}$ and g_{d0i} is the zero-bias drain conductance of M_i, γ_i, δ_i and κ_i are the noise parameters of M_i [5], [6].

The output noise shown in Fig. 5 is calculated from Eq. (21) as

$$\overline{|i_{o,s,eq}|^2} = \frac{4k_BTR_{eq}\omega_{T1}^2\Delta f}{\omega_0^2(1+\alpha_{gd}M)^2(R_{eq}+R_{in})^2(1+1/g_{m2}R_I)^2}. \tag{24}$$

From Eqs. (22) and (23), the equation of the output noise due to M_1 shown in Fig. 5 is derived as

$$\overline{|i_{o,M_1}|^2} = \frac{4k_BT\gamma_1\chi_1 g_{m1}(R_{eq}+r_{nqs,eff})^2\Delta f}{\alpha_1(R_{eq}+R_{in})^2(1+1/g_{m2}R_I)^2}, \tag{25}$$

$$\chi_1 = 1-\frac{2|c|\alpha_1 R_{eq}}{(1+\alpha_{gd}M)(R_{eq}+r_{nqs,eff})}\sqrt{\frac{\delta_1}{\kappa_1\gamma_1}} + \frac{\delta_1\alpha_1^2}{\kappa_1\gamma_1}\frac{R_{eq}^2+1/\omega_0^2C_{gs1,eff}^2}{(1+\alpha_{gd}M)^2(R_{eq}+r_{nqs,eff})^2} \tag{26}$$

where $c \simeq j0.395$ is the correlation coefficient between the induced-gate and drain noise currents [5], [6]. The detailed derivations are summarized in the Appendix.

Figure 6 shows the noise equivalent circuit of the common-gate stage of the LNA. The noise current $i_{nR_{L_i}}$ originating from the internal or load LC tank is given by

$$\overline{|i_{nR_{L_i}}|^2} = \frac{4k_BT\Delta f}{R_{L_i,p}}. \tag{27}$$

The detailed derivations of the output noise due to M_2 are also summarized in the Appendix. The output noise originating from M_2 is given by

$$\overline{|i_{o,M_2}|^2} = 4k_BT\frac{\gamma_2}{\alpha_2}\chi_2 g_{m2}\Delta f, \tag{28}$$

$$\chi_2 = \frac{1}{(1+g_{m2}R_I)^2} + \frac{1}{(1+1/g_{m2}R_I)^2}\left(\frac{\omega_0}{\omega_{T2}}\right)^2\frac{\alpha_2^2\delta_2}{\kappa_2\gamma_2}. \tag{29}$$

The output noises due to the internal and load LC tanks shown in Fig. 6 are derived from Eq. (27) as

$$\overline{|i_{o,R_I}|^2} = \frac{4k_BT\Delta f}{(1+1/g_{m2}R_I)^2R_I}, \tag{30}$$

$$\overline{|i_{o,R_{L_3}}|^2} = \overline{|i_{nR_{L_3}}|^2} = \frac{4k_BT\Delta f}{R_{L_3,p}}. \tag{31}$$

Therefore, NF of the two-stage LNA results in

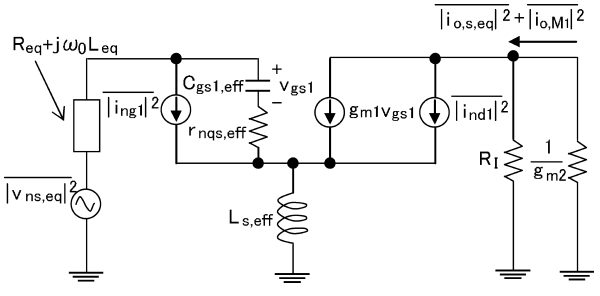

Fig. 5 Noise equivalent circuit of input stage.

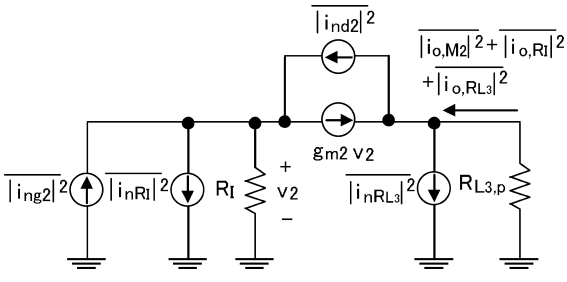

Fig. 6 Noise quivalent circuit of common-gate stage.

$$NF = \frac{\overline{|i_{o,s,eq}|^2} + \overline{|i_{o,M_1}|^2} + \overline{|i_{o,M_2}|^2} + \overline{|i_{o,R_I}|^2} + \overline{|i_{o,R_{L_3}}|^2}}{\overline{|i_{o,s,eq}|^2}}$$
$$= 1 + \frac{\gamma_1\chi_1}{\alpha_1}\left(\frac{\omega_0}{\omega_{T1}}\right)^2 \frac{g_{m1}(1+\alpha_{gd}M)^2(R_{eq}+r_{nqs,eff})^2}{R_{eq}}$$
$$+ \left(\frac{\omega_0}{\omega_{T1}}\right)^2 \frac{(1+\alpha_{gd}M)^2(R_{eq}+R_{in})^2}{R_{eq}}\left(1+\frac{1}{g_{m2}R_I}\right)^2$$
$$\times\left[\frac{\gamma_2\chi_2 g_{m2}}{\alpha_2} + \frac{1}{(1+1/g_{m2}R_I)^2 R_I} + \frac{1}{R_{L_{3,p}}}\right]. \quad (32)$$

4.3 IIP_3

The output of a non-linear small-signal amplifier $y(t)$ is approximately expressed as

$$y(t) \approx a_1 x(t) + a_2 x^2(t) + a_3 x^3(t) \quad (33)$$

where $x(t)$ is an input signal. The IIP_3 of the amplifier in the expression of voltage amplitude is given by [9]

$$A_{IIP_3} = \sqrt{\frac{4}{3}\left|\frac{a_1}{a_3}\right|}. \quad (34)$$

IIP_3 usually expressed as the available power of signal source is given by

$$IIP_3 = \frac{A^2_{IIP_3}}{8R_s}. \quad (35)$$

The overall $A^2_{IIP_3}$ of the LNA consisting of the input and the output stages (Fig. 2) is given by [9]

$$\frac{1}{A^2_{LNA,IIP_3}} \simeq \frac{1}{A^2_{1,IIP_3}} + \frac{A^2_{v1}}{A^2_{2,IIP_3}} \quad (36)$$

where A_{1,IIP_3} and A_{2,IIP_3} represent the IIP_3 of the input and output stages in the expression of voltage amplitude, respectively. A_{v1} is the voltage gain of the input stage, which is given by

$$A_{v1} = \left|\frac{g_{m1}\left(\frac{1}{g_{m2}} // R_I\right)}{j\omega_0 C_{gs1,eff}(R_{eq}+R_{in})(1-\omega_0^2 C_p L_g + j\omega_0 C_p R_s)}\right|. \quad (37)$$

The drain current of MOSFET at each stage is expressed as [10]

$$I_{di} = \frac{1}{2}\mu_0 C_{ox}\frac{W_i}{L}\frac{V^2_{odi}}{1+\Theta V_{odi}}\frac{1}{1-\lambda V_{dsi}} \quad (38)$$

where W_i and L are the gate width and length of M_i, λ is the channel-length modulation coefficient, $\Theta = \mu_0/(2v_{sat}L) + \theta$, v_{sat} the saturation velocity of the carrier, μ_0 the carrier mobility under low electric field and θ the mobility reduction parameter. From Eq. (38), for a signal $v_s(t)$ applied to the LNA, the output current of each stage is derived as

$$I_{di}(t) = \frac{c_0(c_1 + c' v_i(t))^2}{c_2 + c_3 v_i(t) + c'^2 c_4 v_i^2(t)} \quad (i = 1, \ 2), \quad (39)$$

$$c' = \frac{1}{j\omega_0 C_{gs1,eff}(R_{eq}+R_{in})} \times \frac{1}{1-\omega_0^2 L_g C_p + j\omega_0 C_p R_s} \quad (i = 1), \quad (40)$$

$$-1 \quad (i = 2), \quad (41)$$

$$c_0 = \frac{1}{2}\mu_0 C_{ox}\frac{W_i}{L}, \quad (42)$$

$$c_1 = V_{odi}, \quad (43)$$

$$c_2 = (1 + \Theta V_{odi})(1 - \lambda V_{dsi}), \quad (44)$$

$$c_3 = (1 + \Theta V_{odi})\lambda A_{vi} + c'(1 - \lambda V_{dsi})\Theta, \quad (45)$$

$$c_4 = \Theta\lambda A_{vi} \quad (46)$$

where $v_1(t) = v_s(t)$ and $v_2(t) = -A_{v1}v_s(t)$. In the derivation of Eqs. (39)–(46), the channel-length modulation in M_1 due to the variation of the source voltage is neglected. Substituting Taylor expansion coefficients of Eq. (39), a_1 and a_3, into Eq. (34), $A^2_{IIP_3}$ of each stage can be derived as

$$A^2_{i,IIP_3} = \frac{4}{3}\left|\frac{c_1 c_2^2(c_1 c_3 - 2c' c_2)}{(-c' c_2 + c_1 c_3)[(-c' c_2 + c_1 c_3)c_3 - 2c' c_1 c_2 c_4]}\right|. \quad (47)$$

The overall IIP_3 of the LNA can be given by Eqs. (35), (36) and (47).

5. Design of the Two-Stage LNA

The transconductance of M_i is a derivative of Eq. (38), which is given by

$$g_{mi} = \frac{1}{2}\mu_0 C_{ox}\frac{W_i}{L}\frac{V_{odi}(2+\Theta V_{odi})}{(1+\Theta V_{odi})^2}\frac{1}{1-\lambda V_{dsi}}. \quad (48)$$

The power gain, NF and IIP_3 are expressed as a function of V_{odi} by using Eq. (48) and the equations derived in the previous section. In what follows, we discuss a design methodology of the two-stage LNA with those parameters. In NF calculation, the noise paprameter, γ_i and δ_i of a 1-V LNA in 0.15-μm FD-SOI CMOS technology based on the experimental results [11] are used.

The specifications of LNA are shown in Table 1. These are typical specifications for the LNA of a wireless local area network (WLAN) receiver.

(1) Gate lengths of M_1 and M_2

The gate length chosen is the minimum length of 0.14 μm because NF decreases with scaling the gate length [5], [6].

(2) Input impedance

The input impedance of LNA, R'_{in}, is designed to be lower than R_s in such a way that both the power gain and NF improve [4]. For simplicity, R'_{in} is set to R_s.

(3) Bias currents of M_1 and M_2

Table 1 Specifications of LNA.

Operation frequency	5.4 GHz
S_{11}	< -10 dB
Power Gain	> 20 dB
NF	< 2.0 dB
Current Consumption	8.0 mA
Supply Voltage	1.0 V

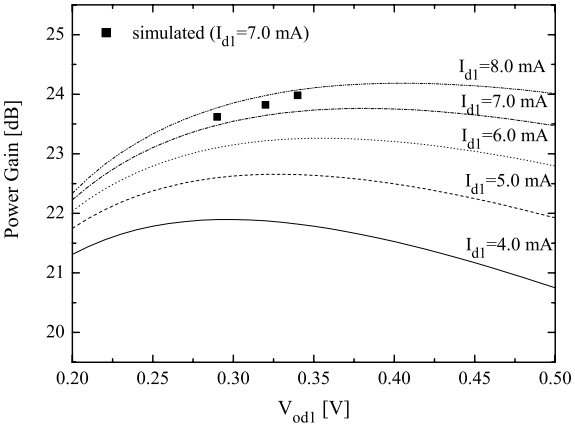

Fig. 7 Calculated and simulated power gain versus V_{od1}.

Equation (20) shows that the common-gate stage has a small influence on the overall power gain. Therefore, the bais current of M_1, I_{d1}, is chosen to satisfy the power gain specification.

Figure 7 shows the calculated power gain versus V_{od1} as a parameter of I_{d1}. Note that g_{m2} is set to infinity in Eq. (20). For comparison, simulated results ($I_{d1} = 7.0$ mA) are also plotted in the figure. This and the following simulations of the LNA are carried out using the small-signal and noise FD-SOI MOS device model [11]. The calculated results are comparable to the simulated ones. The given specification is satisfied in the range of 4.0–8.0 mA. Taking account of process and temperature variations, we choose I_{d1} to be 7.0 mA for a power gain of 23 dB including a 3 dB margin and $I_{d2} = 1.0$ mA from the power specification.

(4) Overdrive of M_1

For NF and IIP3 of the input stage, $\overline{|i_{o,M_2}|^2}$ and g_{m2} are set to 0 and infinity in Eq. (32), respectively, and A^2_{2,IIP_3} to infinity in Eq. (36). Figure 8 shows the calculated and simulated NF and IIP_3 versus V_{od1} at $I_{d1} = 7.0$ mA. Again, the calculated results are comparable to the simulated ones.

From the figure, the increase of V_{od1} results in better noise performance of the LNA, but poor linearity. The degradation of linearity can be explained as follows: Under the impedance matching condition, the constant current $i_{in} = v_s/2R_s$ injects in the LNA. The small-signal voltage of gate-source of M_1 is given by

$$v_{gs1} \simeq \frac{i_{in}}{j\omega_0 C_{gs1}}. \tag{49}$$

The gate-source capacitance of M_1, C_{gs1}, decreases with increasing V_{od1} under constant I_{d1}, resulting in the increase

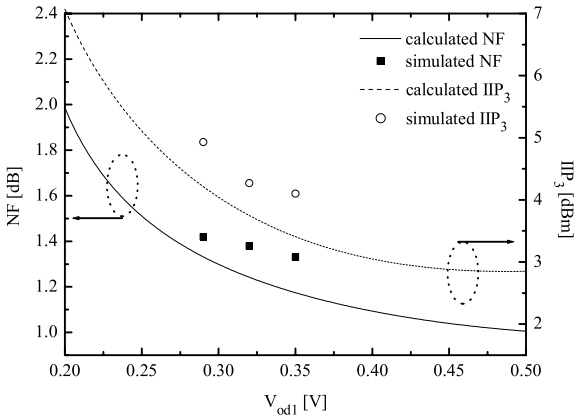

Fig. 8 Calculated and simulated NF and IIP_3 versus V_{od1}.

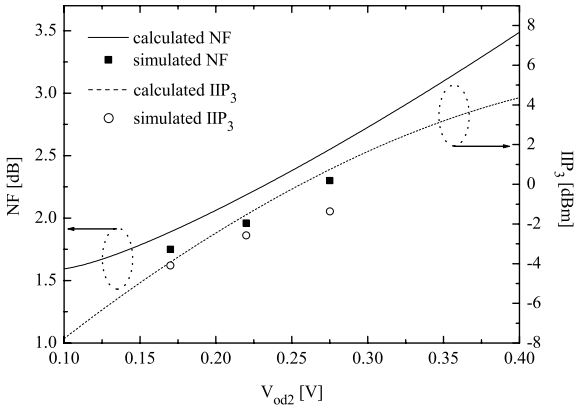

Fig. 9 Calculated and simulated NF and IIP_3 versus V_{od2}.

of v_{gs1}. Although the MOSFET generally has higher linearity with increasing V_{od1}, in the range of 0.20–0.50 V, the degradation of linearity due to the increase in v_{gs1} becomes significant, causing poor linearity. Therefore, a smaller V_{od1} results in an LNA with higher linearity. Taking account of an additional noise of the output stage, we choose $V_{od1} = 0.32$ V, resulting in $W_1 = 120\,\mu$m.

(5) Overdrive of M_2

Figure 9 shows the calculated and simulated NF and IIP_3 versus V_{od2} at $I_{d1} = 7.0$ mA, $V_{od1} = 0.32$ V and $I_{d2} = 1.0$ mA. The differences between the simulated and calculated results at a higher V_{od2} originate form the simplified noise equivalent circuit including the Miller effect (Fig. 5) and the IIP_3 approximation of two non-linear stages in cascade (Eq. (36)).

Although the increase of V_{od1} results in better noise performance and poor linearity as shown in Fig. 8, the increase of V_{od2} leads to the opposite results: Better linearity and poor noise performance. This is because decreasing g_{m2} increases the Miller factor M, resulting in a higher NF. Therefore, an LNA with both the given noise performance and high linearity can be achieved by choosing the highest V_{od2}, that is, 0.17 V satisfying the NF specification, resulting in $W_2 = 50\,\mu$m.

(6) Inductors and capacitors

Substituting the determined parameters into the equation of L_g derived from Eqs. (2), (3), (11), (15) and (16), $L_g = 3.3$ nH is derived and then $L_s = 1.0$ nH from Eqs. (3) and (16).

Finally, the resonance condition gives inductors L_i of 3.1 nH and capacitors C_i of 120 fF (i =1, 2, 3). We used the ac-coupling capacitor C_c of 3.3 pF which is large enough not to affect RF signals.

From the above consideration, the following performances are expected: The power gain of 23 dB, NF 1.8 dB, IIP_3 −4.1 dBm and power consumption 8 mW.

6. Experimental Results

A two-stage LNA is implemented in a 0.15-μm FD-SOI CMOS process with five metal layers and metal-insulator-metal (MIM) capacitors. The cut-off frequency of a 0.15 μm NMOS consisting of 48 fingers with a unit of 5 μm width is about 54 GHz at $V_{ds} = 1$ V and $I_d = 7$ mA [1]. The microphotograph of the fabricated LNA is shown in Fig. 10. All the pads are not ESD protected. A quality factor of on-chip inductors is about 11 at 5.4 GHz. The chip area is 0.78 mm × 0.73 mm. For the measurement, a buffer with a voltage gain of around 0 dB is implemented. The buffer has a small influence on the input reflection and noise performance of the LNA because the LNA has high reverse isolation and high gain. The current consumption of the LNA without the buffer is 8.3 mA at a 1-V supply voltage.

S-parameters, NF and IIP_3 of the LNA are measured using on-wafer RF probes. The above characteristics of the LNA with an ideal inductor L_g in series to the gate are calculated based on the measured data [11]. This avoids instrumental error originating from bonding wires.

Figure 11 shows measured and simulated S_{11} and S_{21}, i.e., power gain of the LNA. The impedance matching is achieved ($S_{11} < -10$ dB) around 5.4 GHz where the power gain is 23 dB. Figure 12 shows measured and simulated NF versus frequency. An NF of 1.7 dB is obtained at 5.4 GHz. The measured results agree well with those simulated by the the small-signal and noise model [11].

Figure 13 shows the measured output power of fundamental tone and third-order intermodulation (IM3) products for two tones (5.4 and 5.41 GHz). The measured IIP_3 is about −18.0 dBm. This result includes the nonlinearity of the buffer, which can be eliminated by using the follow equation:

$$\frac{1}{A^2_{LNA,IIP_3}} \simeq \frac{1}{A^2_{LNA+Buf,IIP_3}} - \frac{A^2_{v,LNA}}{A^2_{Buf,IIP_3}} \tag{50}$$

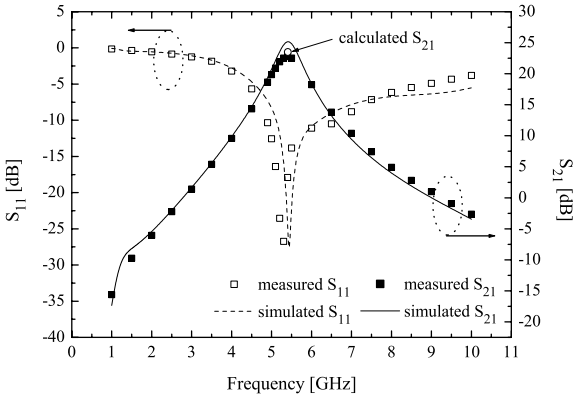

Fig. 11 Measured and simulated S_{11} and S_{21} of LNA.

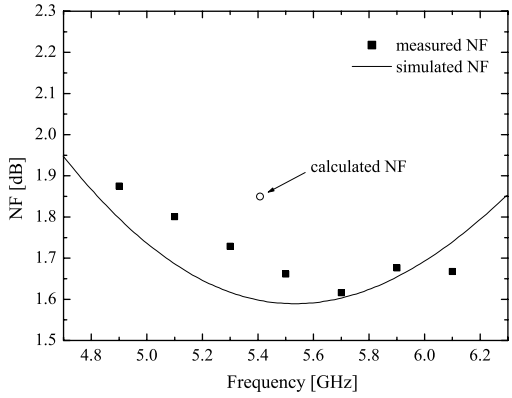

Fig. 12 Measured and simulated NF of LNA.

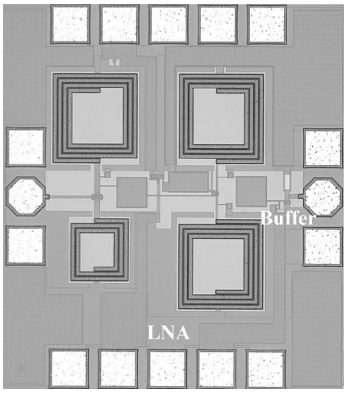

Fig. 10 Microphotograph of LNA.

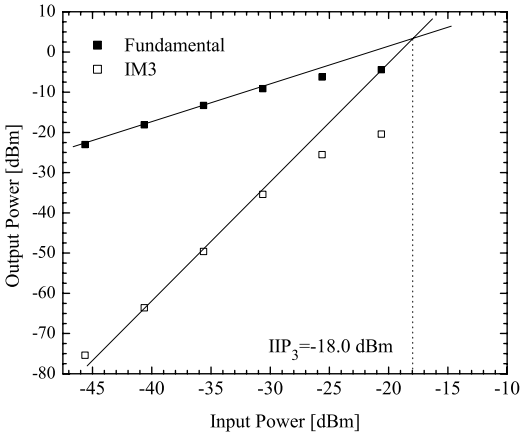

Fig. 13 Measured IIP_3 of LNA including buffer.

Table 2 Comparison of performances of LNA.

	Specification	Measurement	Calculation	Simulation
Power Gain @ 5.4 GHz	20 dB	23 dB	23 dB	25 dB
NF @ 5.4 GHz	2.0 dB	1.7 dB	1.8 dB	1.6 dB
IIP_3	N/A	−6.1 dBm	−4.1 dBm	−3.0 dBm

Table 3 Measured performance of two LNAs.

	L_s=1.0 nH	L_s=0.8 nH
S_{11}	< −10 dB	
Power Gain @ 5.4 GHz	23 dB	26 dB
NF @ 5.4 GHz	1.7 dB	1.4 dB
IIP_3	−6.1 dBm	−7.0 dBm
Current Consumption	8.3 mA	
Supply Voltage	1.0 V	

where $A_{v,LNA}$ is the voltage gain of the LNA, A_{LNA,IIP_3}, A_{Buf,IIP_3} and $A_{LNA+Buf,IIP_3}$ represent the IIP_3 of the LNA, buffer and LNA including the buffer in the expression of voltage amplitude, respectively. Substituting measured $IIP_{3,LNA+Buf} = -18.0$ dBm, $IIP_{3,Buf} = 10.8$ dBm and $A_{v,LNA} = 22.5$ dB into Eq. (50), the IIP_3 of the LNA is achieved about −6.1 dBm.

Among other characteristics, S_{12} and S_{22} are below −42 dB and −10 dB, respectively.

Table 2 shows a comparison of performances of the LNA. The simulated and calculated power gain and NF are consistent with the measured results and the fabricated LNA, thus satisfying the specifications. The calculated IIP_3 agrees with the simulated one, but these results are slightly different from the measured IIP_3. The difference is due to inaccurate FD-SOI MOS device parameters used in the simulation and calculation.

Table 3 shows a performance summary of the above LNA (L_s = 1.0 nH) and other fabricated LNA with L_s = 0.8 nH. The table suggests that power gain and noise performance of the LNA can be improved by lowering L_s.

7. Conclusion

We investigated high frequency characteristics of a low-voltage two-stage CMOS LNA. Based on the derived equations of power gain, NF and IIP_3, we proposed a new design methodology of the LNA. By using the overdrive voltages of the MOSFETs as adjustable parameters, we demonstrated systematic design of an LNA under given specifications. A 1-V 5.4-GHz LNA was realized in 0.15-μm FD-SOI CMOS technology. The LNA achieved a power gain of 23 dB, NF of 1.7 dB and IIP_3 of −6.1 dBm with a power consumption of 8.3 mW. The results are consistent with the calculated results obtained from the derived equations. This ensures the validity of the equations and proposed design methodology.

Acknowledgements

This study is supported by Semiconductor Technology Academic Research Center (STARC). The chip design in this work is also supported by VLSI Design and Education Center (VDEC), the University of Tokyo in collaboration with Synopsys, Inc., Cadence Design System, Inc. and Agilent Technologies Japan, Ltd.

References

[1] F. Ichikawa, Y. Nagatomo, Y. Katakura, M. Itoh, S. Itoh, H. Matsuhashi, T. Ichimori, N. Hirashita, and S. Baba, "Fully depleted SOI process and technology for digital and RF applications," Solid-State Electron., vol.48, pp.999–1006, 2004.
[2] A.O. Adan, T. Yoshimatsu, S. Shitara, N. Tanba, and M. Fukumi, "Linearity and low-noise performance of SOI MOSFETs for RF applications," IEEE Trans. Electron Devices, vol.49, no.5, pp.881–888, May 2002.
[3] M. Brandolini, P. Rossi, D. Manstretta, and F. Svelto, "Toward multistandard mobile terminals-fully integrated receivers requirements and architecures," IEEE Trans. Microw. Theory Tech., vol.53, no.3, pp.1026–1038, March 2005.
[4] J. Janssens and M. Steyaert, CMOS Cellular Receiver Front-Ends: From Specification to Realization, Kluwer Academic Publishers, Boston, 2002.
[5] D.K. Shaeffer and T.H. Lee, "A 1.5-V, 1.5-GHz CMOS low noise amplifier," IEEE J. Solid-State Circuits, vol.32, no.5, pp.745–759, May 1997.
[6] D.K. Shaeffer and T.H. Lee, "Corrections to "A 1.5-V, 1.5-GHz CMOS low noise amplifier,"" IEEE J. Solid-State Circuits, vol.40, no.6, pp.1397–1398, June 2005.
[7] T. Kihara, G. Kim, Y. Shimizu, B. Murakami, K. Ueda, M. Goto, T. Matsuoka, and K. Taniguchi, "Design of CMOS low-noise amplifier considering noise and linearity," IEICE Trans. Electron. (Japanese Edition), vol.J89-C, no.2, pp.72–75, Feb. 2006.
[8] C.L. Hsiao, R.M. Weng, K.Y. Lin, and H.C. Wei, "A sub 1 V 2.4 GHz CMOS variable-gain low noise amplifier," IEICE Trans. Electron., vol.E87-C, no.6, pp.1003–1004, June 2004.
[9] B. Razavi, RF Microelectronics, Prentice Hall PTR, New Jersey, 1998.
[10] B. Razavi, Design of Analog CMOS Integrated Circuits, McGraw-Hill, New York, 2001.
[11] G. Kim, B. Murakami, M. Goto, T. Kihara, K. Nakamura, Y. Shimizu, T. Matsuoka, and K. Taniguchi, "Small-signal and noise model of FD-SOI MOS devices for low noise amplifier," Jpn. J. Appl. Phys., Pt.1, vol.45, no.9A, pp.6872–6877, Sept. 2006.

Appendix: Derivations of Output Noise Originating from M_1 and M_2

The induced-gate noise correlates to the drain noise. Considering the correlation between the gate and drain noises, the induced-gate noise is expressed as the sum of correlated and uncorrelated components:

$$\begin{aligned}\overline{|i_{ng}|^2} &= \overline{|i_{ngc}|^2} + \overline{|i_{ngu}|^2} \\ &= \overline{|i_{ng}|^2}|c|^2 + \overline{|i_{ng}|^2}(1-|c|^2)\end{aligned} \quad (\text{A}\cdot 1)$$

where i_{ng} is given by Eq. (23). The correlation coefficient, c, between the induced-gate and drain noise currents is given

by [5], [6]

$$c = \frac{\overline{i_{ng} \cdot i_{nd}^*}}{\sqrt{\overline{|i_{ng}|^2}}\sqrt{\overline{|i_{nd}|^2}}}. \quad (\text{A}\cdot 2)$$

From the correlation shown above, the output noise due to M_i is expressed as

$$\begin{aligned}\overline{|i_{o,M_i}|^2} &= \overline{|i_{o,ndi} + i_{o,ngi}|^2} \\ &= \overline{|i_{o,ndi} + i_{o,ngci}|^2} + \overline{|i_{o,ngui}|^2} \\ &= \overline{|i_{o,ndi}|^2} + \overline{i_{o,ngci} \cdot i_{o,ndi}^*} + \overline{i_{o,ndi} \cdot i_{o,ngci}^*} \\ &\quad + \overline{|i_{o,ngci}|^2} + \overline{|i_{o,ngui}|^2}, \end{aligned} \quad (\text{A}\cdot 3)$$

where $i_{o,ndi}$, $i_{o,ngci}$ and $i_{o,ngui}$ are the output noise currents originating from i_{ndi}, i_{ngci} and i_{ngui}, respectively.

From Fig. 5, the transfer function from the drain noise current i_{nd1} to the output $i_{o,nd1}$ is given by

$$H_{nd1}(j\omega_0) = \frac{R_{eq} + r_{nqs,eff}}{(R_{eq} + R_{in})(1+1/g_{m2}R_I)}. \quad (\text{A}\cdot 4)$$

The transfer function from the induced-gate noise current i_{ng1} to the output $i_{o,ng1}$ is also given by

$$H_{ng1}(j\omega_0) = \frac{\omega_{T1}\left(R_{eq} + j/\omega_0 C_{gs1,eff}\right)}{j\omega_0(1+\alpha_{gd}M)(R_{eq}+R_{in})(1+1/g_{m2}R_I)}. \quad (\text{A}\cdot 5)$$

Using Eqs. (22), (23), (A· 4) and (A· 5), we have

$$\begin{aligned}\overline{|i_{o,nd1}|^2} &= |H_{nd1}(j\omega_0)|^2\,\overline{|i_{nd1}|^2} \\ &= \frac{4k_BT\gamma_1 g_{m1}(R_{eq}+r_{nqs,eff})^2\Delta f}{\alpha_1(R_{eq}+R_{in})^2(1+1/g_{m2}R_I)^2}, \end{aligned} \quad (\text{A}\cdot 6)$$

$$\begin{aligned}&\overline{i_{o,ngc1}\cdot i_{o,nd1}^*} + \overline{i_{o,nd1}\cdot i_{o,ngc1}^*} \\ &= H_{ngc1}(j\omega_0) i_{ngc1}\cdot H_{nd1}^*(j\omega_0) i_{nd1}^* \\ &\quad + H_{nd1}(j\omega_0) i_{nd1}\cdot H_{ngc1}^*(j\omega_0) i_{ngc1}^* \\ &= -2|c|\sqrt{\frac{\delta_1}{\kappa_1\gamma_1}}\frac{4k_BT\gamma_1 g_{m1}R_{eq}(R_{eq}+r_{nqs,eff})\Delta f}{(1+\alpha_{gd}M)(R_{eq}+R_{in})^2(1+1/g_{m2}R_I)^2}, \end{aligned} \quad (\text{A}\cdot 7)$$

$$\begin{aligned}&\overline{|i_{o,ngc1}|^2} + \overline{|i_{o,ngu1}|^2} \\ &= \left|H_{ng1}(j\omega_0)\right|^2\overline{|i_{ng1}|^2} \\ &= \frac{4k_BT\alpha_1\delta_1 g_{m1}(R_{eq}^2+1/\omega_0^2 C_{gs1,eff}^2)\Delta f}{\kappa_1(1+\alpha_{gd}M)^2(R_{eq}+R_n)^2(1+1/g_{m2}R_I)^2}. \end{aligned} \quad (\text{A}\cdot 8)$$

Substituting Eqs. (A· 6)–(A· 8) into Eq. (A· 3), Eq. (25) can be derived.

In the same way, the output noise originating from M_2 is also derived. From Fig. 6, the transfer functions from the drain and induced-gate noise currents to the output are derived as

$$H_{nd2}(j\omega_0) = \frac{1}{1+g_{m2}R_I}, \quad (\text{A}\cdot 9)$$

$$H_{ng2}(j\omega_0) = \frac{1}{1+1/g_{m2}R_I}. \quad (\text{A}\cdot 10)$$

From Eqs. (22), (23), (A· 9) and (A· 10), we have

$$\overline{|i_{o,nd2}|^2} = \frac{4k_BT\gamma_2 g_{m2}}{\alpha_2(1+g_{m2}R_I)^2}, \quad (\text{A}\cdot 11)$$

$$\overline{i_{o,ngc2}\cdot i_{o,nd1}^*} + \overline{i_{o,nd2}\cdot i_{o,ngc2}^*} = 0, \quad (\text{A}\cdot 12)$$

$$\overline{|i_{o,ngc2}|^2} + \overline{|i_{o,ngu2}|^2} = \frac{4k_BT\delta_2\alpha_2(\omega_0 C_{gs2})^2}{\kappa_2 g_{m2}(1+1/g_{m2}R_I)^2}. \quad (\text{A}\cdot 13)$$

Substituting Eqs. (A· 11)–(A· 13) into Eq. (A· 3), Eq. (28) can be derived.

Takao Kihara received the B.S. and M.S. degrees in electronic engineering from Osaka University, Osaka, Japan, in 2005 and 2006, respectively. He is now working towards his Ph.D. degree at Osaka University. His current research interests include CMOS RF circuits.

Guechol Kim recevied the B.S. and M.S. degrees in electronic engineering from Mokpo National University, Mokpo, Korea, in 2000 and 2003, respectively. He is now working towards his Ph.D. degree at Osaka University. His current research interests include FD-SOI MOSFET and RF circuits.

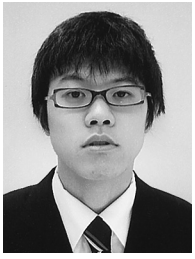

Masaru Goto received the B.S. degree in electronic engineering from Osaka University, Osaka, Japan, in 2005. He is now working towards his M.S degree at Osaka University. His current research interests include CMOS RF circuits.

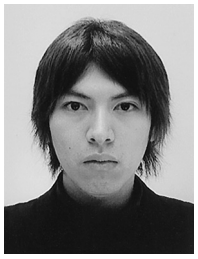

Keiji Nakamura received the B.S. degree in electronic engineering from Osaka University, Osaka, Japan, in 2006. He is now working towards his M.S degree at Osaka University. His current research interests include CMOS RF circuits and phase locked loops.

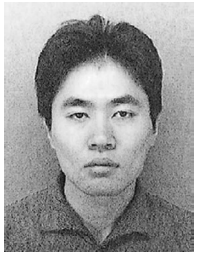

Yoshiyuki Shimizu received the B.S., M.S. and Ph.D. degrees in electronic engineering from Osaka University, Osaka, Japan, in 2000, 2002 and 2005 respectively. He is now a postdoctoral fellow at Osaka University.

Toshimasa Matsuoka received the B.S., M.S. and Ph.D. degrees in electronic engineering from Osaka University, Osaka, Japan, in 1989, 1991 and 1996, respectively. During 1991–1998, he worked for the Central Research Laboratories, Sharp Corporation, Nara, Japan, where he was engaged in the research and development of deep submicron CMOS devices and ultra thin gate oxides. Since 1999, he has been working for Osaka University, where he is Associate Professor now. His current research includes MOS device modeling and CMOS RF circuits. Dr. Matsuoka is a member of the Japan Society of Applied Physics, the IEEJ, and the IEEE.

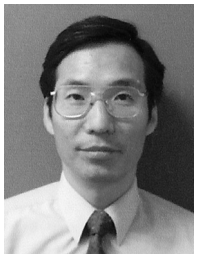

Kenji Taniguchi received the B.S., M.S. and Ph.D. degrees from Osaka University, Osaka, Japan, in 1971, 1973 and 1986, respectively. From 1973 to 1986, he worked for Toshiba Research and Development Center, Kawasaki, Japan where he was engaged in process modeling and the design of MOS LSI fabrication technology. He was a Visiting Scientist at Massachusetts Institute of Technology, Cambridge, from July 1982 to November 1983. Presently, he is a Professor of Electrical, Electronic and Information Engineering at Osaka University. His current research interests are analog circuits, radio frequency circuits, device physics and process technology. Prof. Taniguchi is a member of the Japan Society of Applied Physics. He is a fellow of the IEEE.